

Theoretical study on the mechanism of $C_2Cl_3 + NO_2$ reaction

Yan Li · Hui-ling Liu · Xu-ri Huang · De-quan Wang ·
Chia-chung Sun · Au-chin Tang

Received: 15 October 2008 / Accepted: 16 February 2009 / Published online: 14 March 2009
© Springer-Verlag 2009

Abstract The radical-molecule reaction of C_2Cl_3 with NO_2 is explored at the B3LYP/6-311G(d,p) and CCSD(T)/6-311+G(d,p) (single-point) levels. On the singlet potential energy surface (PES), the association between C_2Cl_3 and NO_2 is found to be carbon-to-nitrogen attack forming the adduct $C_2Cl_3NO_2$ (**1**) without any encounter barrier, followed by isomerization to C_2Cl_3ONO (**2**). Starting from **2**, the most feasible pathway is the N–O1 bond cleavage which lead to P_1 ($C_2Cl_3O + NO$). Much less competitively, **2** transforms to the three-membered ring isomer $c-OCCL_2C-CINO$ (**4^a**) which can easily interconvert to $c-OCCL_2C-CINO$ **4^b**. Then **4** (**4^a**, **4^b**) takes direct C1–C2 and C2–O1 bonds cleavage to give P_2 ($COCl_2 + ClNO$). The lesser competitive channel is the **4^a** isomerizes to the four-membered ring intermediate $O-c-CNClOCCl_2$ (**5**) followed by dissociation to P_3 ($CO + ClNOCCl_2$). The concerted 1,2-Cl shift along with C1–O1 bond rupture of **4^b** to form $ONC(O)CCl_3$ (**6**) followed by dissociation to P_4 ($ClNO + OCCCl_2$) is even much less feasible. Moreover, some of P_3 and P_4 can further dissociate to P_5 ($ClNO + CO + CCl_2$). Compared with the singlet pathways, the triplet pathways may have less contribution to the title reaction. Our results are in marked difference from previous theoretical studies which showed that two initial adducts $C_2Cl_3-NO_2$ and C_2Cl_3-ONO are obtained. Moreover, in the present paper we focus our main attentions on the cyclic isomers in view of only the chain-like isomers are considered by previous studies. The present study may

be helpful for understanding the halogenated vinyl chemistry.

Keywords Theoretical calculations · Reaction mechanism · Potential energy surface (PES) · Trichlorovinyl (C_2Cl_3) · Nitric dioxide (NO_2)

1 Introduction

The pyrolysis and oxidation of chlorinated hydrocarbons (CHCs) are involved in many practical processes, such as inhabiting flame propagation [1] and soot formation in flames [2]. Furthermore, reactions of trichlorovinyl radical, C_2Cl_3 have been demonstrated to be among the most important and sensitive reactions in a number of systems of combustion and pyrolysis of chlorine-rich unsaturated chlorinated hydrocarbons [3, 4]. Due to the above importance, a number of experimental and theoretical studies have been reported on the reactions of C_2Cl_3 radical with O_2 [5–8], Cl_2 [9], NO_2 [10, 11] as well as unimolecular decomposition of C_2Cl_3 [12].

On the other hand, the nitrogen oxides, NO_x are among the major atmosphere pollutants released in combustion processes. To minimize the harmful effects, before their release into the atmosphere, one effective way is to chemically reduce them by reburning the combustion products [13–17]. Up to now, a large number of experimental and theoretical investigations have been devoted to NO_2 reactions with a variety of radicals, such as CH_2F [18], CH_2Cl [19, 20], CH_3 [21–23], $CHCl_2/CCl_3$ [24], CH_2 [25–27], CH [28–31], CF [32, 33], CHF [34, 35], $CHCl$ [36, 37], C_2H_3 [38], N_3 [39], etc.

In 2007, Xiang et al. [10] carried out the experimental studies of the reaction between C_2Cl_3 and NO_2 using the

Y. Li · H.-l. Liu · X.-r. Huang (✉) · D.-q. Wang · C.-c. Sun · A.-c. Tang
State Key Laboratory of Theoretical and Computational Chemistry, Institute of Theoretical Chemistry, Jilin University, 130023 Changchun, People's Republic of China
e-mail: snow2007liyan@163.com

step-scan time-resolved Fourier transform infrared (TR-FTIR) emission spectroscopy and three vibrationally excited reaction products Cl_2CO , CO and NO are observed. In their later study [11] in 2008, they reinvestigated the title reaction by step-scan TR-FTIR emission spectroscopy and electronic structure calculations. Their calculated results can well explain the experimental observations. However, we are aware that only the chain-like intermediates are considered on Xiang et al.'s potential energy surface (PES). That is to say, their calculations are incomplete. Thus, in the present paper, we investigate a detailed theoretical study on the title reaction and we mainly focused on the cyclic isomers and their further changes.

2 Computational methods

All the calculations are performed using the Gaussian 98 program packages [40]. The geometries of reactants, products, intermediates and transition states are optimized using the popular Density Functional Theory B3LYP functions in conjunction with the 6-311G(d,p) basis set. The stationary nature of structures is confirmed by harmonic vibrational frequency calculations, i.e., equilibrium species possess all real frequencies, whereas transition states possess one and only one imaginary frequency. The zero-point energy (ZPE) corrections are obtained at the same level of theory. To confirm that the transition state connects the designated intermediates, intrinsic reaction coordinate (IRC) calculations are performed at the B3LYP/6-311G(d,p) level. In order to get more reliable energetic data, single-point energy calculations are performed at the CCSD(T)/6-311+G(d,p) level using the B3LYP/6-311G(d,p) optimized geometries. Unless otherwise specified, the CCSD(T)/6-311+G(d,p)//B3LYP/6-311G(d,p)+ZPVE energies are used in the following discussion.

To inspect the reliability for result, B3LYP/6-311++G(d,p) and MP2/6-311G(d,p) are used to optimize structures of the most feasible channel followed by CCSD(T) single-point energy calculations. Also, the composite method, G3MP2 is performed to get more reliable results.

3 Results and discussion

The optimized structures of reactant and products are shown in Fig. 1. The optimized structures of intermediates and transition states are shown in Figs. 2 and 3, respectively. The symbol **TSm/n** is used to denote the transition state connecting isomers **m** and **n**. To make our discussion easier, the energy of reactant **R** ($\text{C}_2\text{Cl}_3 + \text{NO}_2$) is set to be zero for reference. Table 1 displays the relative energies

including ZPE corrections of all species at the CCSD(T)/6-311+G(d,p)//B3LYP/6-311G(d,p) level. By means of the transition states and their connected intermediates or products, a schematic PES for $\text{C}_2\text{Cl}_3 + \text{NO}_2$ reaction is plotted in Fig. 4. Moreover, the optimized geometries at MP2/6-311G(d,p) and B3LYP/6-311++G(d,p) levels of the species involved in the most relevant channels are shown in Fig. 5, while the comparative energetic data calculated at various levels are listed in Table 2.

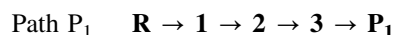
3.1 Initial association

The C_2Cl_3 radical has C_s symmetry and $2A'$ state, the spin density of C atom with only one Cl atom is 0.891274e, so this C atom is the most reactive site. Therefore, the initial association with NO_2 mainly focuses on this C-site. Both singlet and triplet PES can be obtained for the radical-molecule reaction of C_2Cl_3 (C_s , $2A'$) + NO_2 (C_{2v} , 2A_1). On the singlet PES, the carbon-to-nitrogen approach is rather attractive to form structure $\text{C}_2\text{Cl}_3\text{NO}_2$ (**1**) without any encounter barrier. For the carbon-to-oxygen approach, we are unable to find the transition state linking reactant ($\text{C}_2\text{Cl}_3 + \text{NO}_2$) and the intermediate $\text{C}_2\text{Cl}_3\text{ONO}$ (**2**) despite numerous attempts. Yet, we expect that considerable barrier is needed to activate the short N=O double bond (1.194 Å) in NO_2 to form the long N–O weak bond in **2** (1.687 Å). As a result, the carbon (with one Cl atom)-to-nitrogen approach forming isomer **1** is the entrance pathway on singlet PES. **1** lies 56.2 kcal/mol below the reactant, which means that the association is fast and will play a significant role in the reaction kinetics. On the triplet PES, the carbon-to-nitrogen approach can lead to $\text{C}_2\text{Cl}_3\text{NO}_2$ (${}^3\mathbf{1}$) via ${}^3\text{TSR}/\mathbf{1}$ with a high barrier 23.8 kcal/mol with respect to **R** ($\text{C}_2\text{Cl}_3 + \text{NO}_2$). And the barrier of carbon-to-oxygen approach is calculated to be at least 23.3 kcal/mol. In view of the much higher entrance barriers, the triplet pathways may contribute less to the $\text{C}_2\text{Cl}_3 + \text{NO}_2$ reaction compared with the singlet pathways, and thus will not be discussed further. In the following section, we mainly discuss the formation pathways of various products proceeded via $\text{C}_2\text{Cl}_3\text{NO}_2$ (**1**) on the singlet PES.

3.2 Isomerization and dissociation pathways

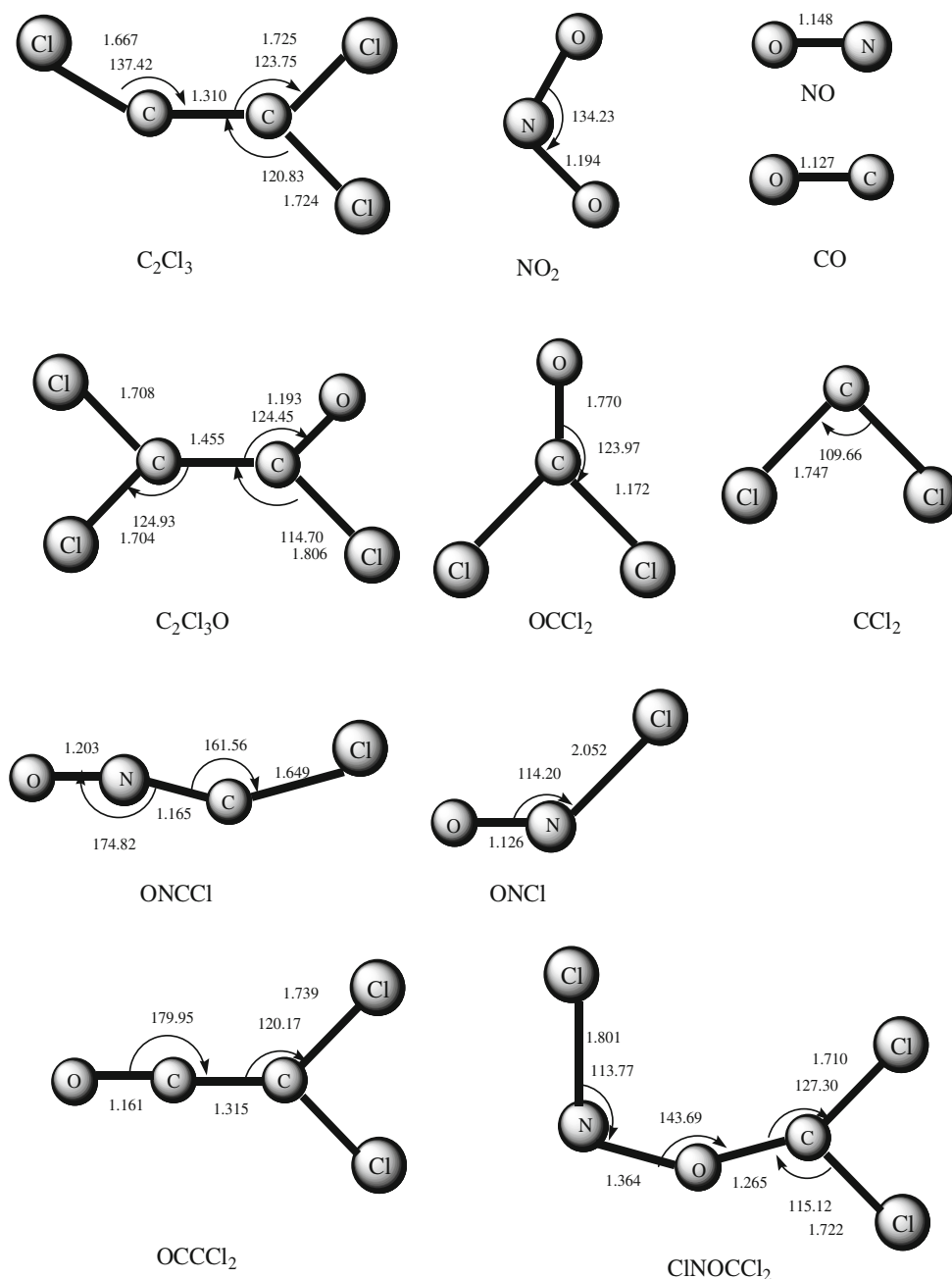
1. Formation pathway of **P₁** ($\text{C}_2\text{Cl}_3\text{O} + \text{NO}$)

From Fig. 4, we find that only one pathway is energetically possible to form **P₁**. It can be written as



The initial adduct $\text{C}_2\text{Cl}_3\text{NO}_2$ (**1**) takes concerted C2–O1 bond formation accompanied by C2–N bond rupture to

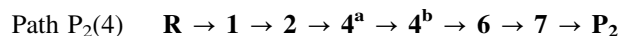
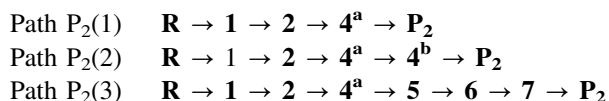
Fig. 1 The optimized structures of reactants and products at the B3LYP/6-311G(d,p) level. Distances are given in angstroms and angles in degrees



form C_2Cl_3ONO (**2**), followed by N–O1 bond rupture to form the weakly bond complex $C_2Cl_3O\dots NO$ (**3**) before the final product P_1 . The barriers for **1** \rightarrow **2** and **2** \rightarrow **3** conversions are 53.1 and 6.1 kcal/mol, respectively.

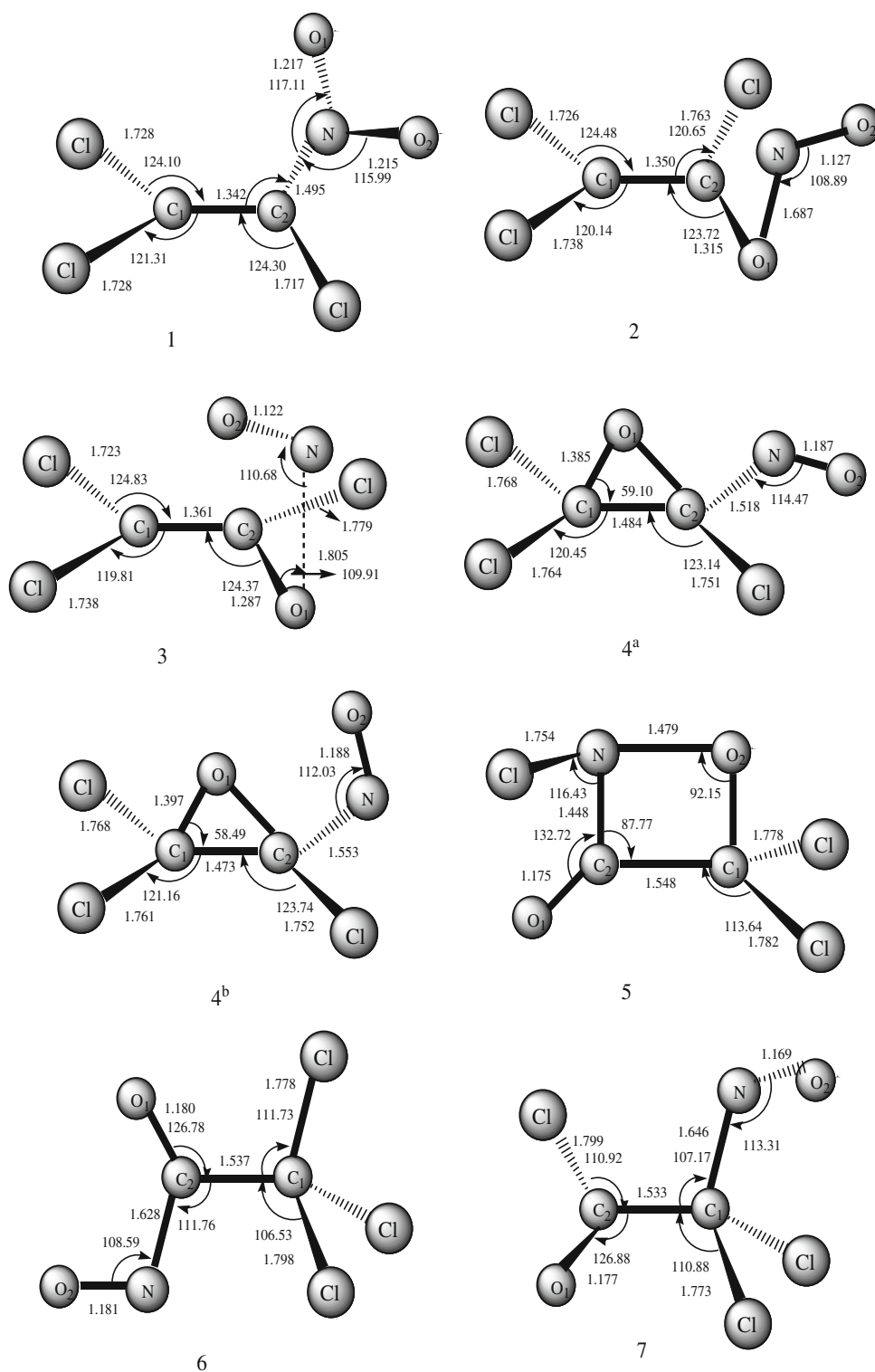
2. Formation pathways of P_2 ($COCl_2 + ClCNO$)

There are four feasible pathways to form P_2 , which can be written as follows:



The formation of C_2Cl_3ONO (**2**) is the same as that in path P_1 . Subsequently, **2** undergoes a concerted C1–O1 bond formation, O1–N bond rupture and C2–N bond formation process to form the three-membered ring intermediate $c\text{-}OCCl_2C\text{-}ClNO$ (4^a), which can transform to 4^b easily. Cleavage of C1–C2 and O1–C2 bonds of 4^a or 4^b can lead to P_2 as in path $P_2(1)$ and path $P_2(2)$. In path $P_2(3)$, 4^a undergoes a concerted Cl-shift (from C2 to N), C1–O1 bond rupture and C1–O2 bond formation process to form the four-membered ring intermediate $O\text{-}c\text{N}ClOCCl_2$

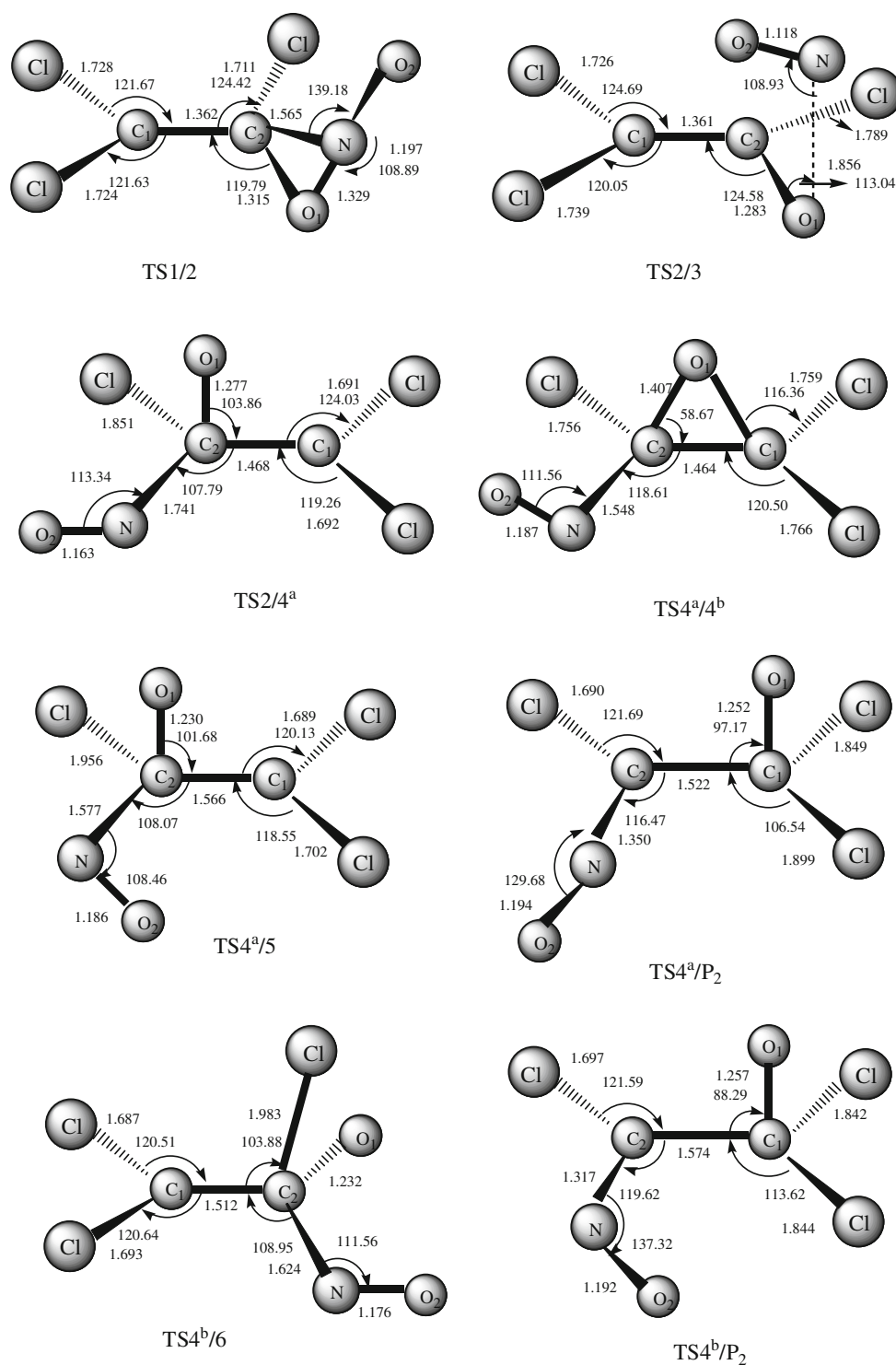
Fig. 2 The optimized structures of the intermediates at the B3LYP/6-311G(d,p) level. Distances are given in angstroms and angles in degrees



(5), followed by a 1,3-Cl-shift along with C1–O2 bond rupture to generate ONC(O)CCl_3 (6). Alternatively, intermediate 6 can be formed via 4^b through a 1,2 Cl-shift accompanied by C1–O1 bond rupture process as in path $P_2(4)$. Finally, 6 isomerizes to $\text{ClC(O)CCl}_2\text{NO}$ (7) followed by the dissociation to P_2 .

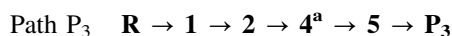
For these four channels, path $P_2(1)$ and path $P_2(2)$ involves fewer intermediates. Also, the energy barriers of $4^b \rightarrow \text{P}_2$ [in path $P_2(2)$], $4^a \rightarrow \text{P}_2$ [in path $P_2(2)$], $7 \rightarrow \text{P}_2$ [in path $P_2(3-4)$] are increase in sequence as 29.0, 38.0 and 57.5 kcal/mol. Therefore, path $P_2(2)$ is expected to be the most feasible channel for P_2 .

Fig. 3 The optimized structures of the transition states at the B3LYP/6-311G(d,p) level. Distances are given in angstroms and angles in degrees



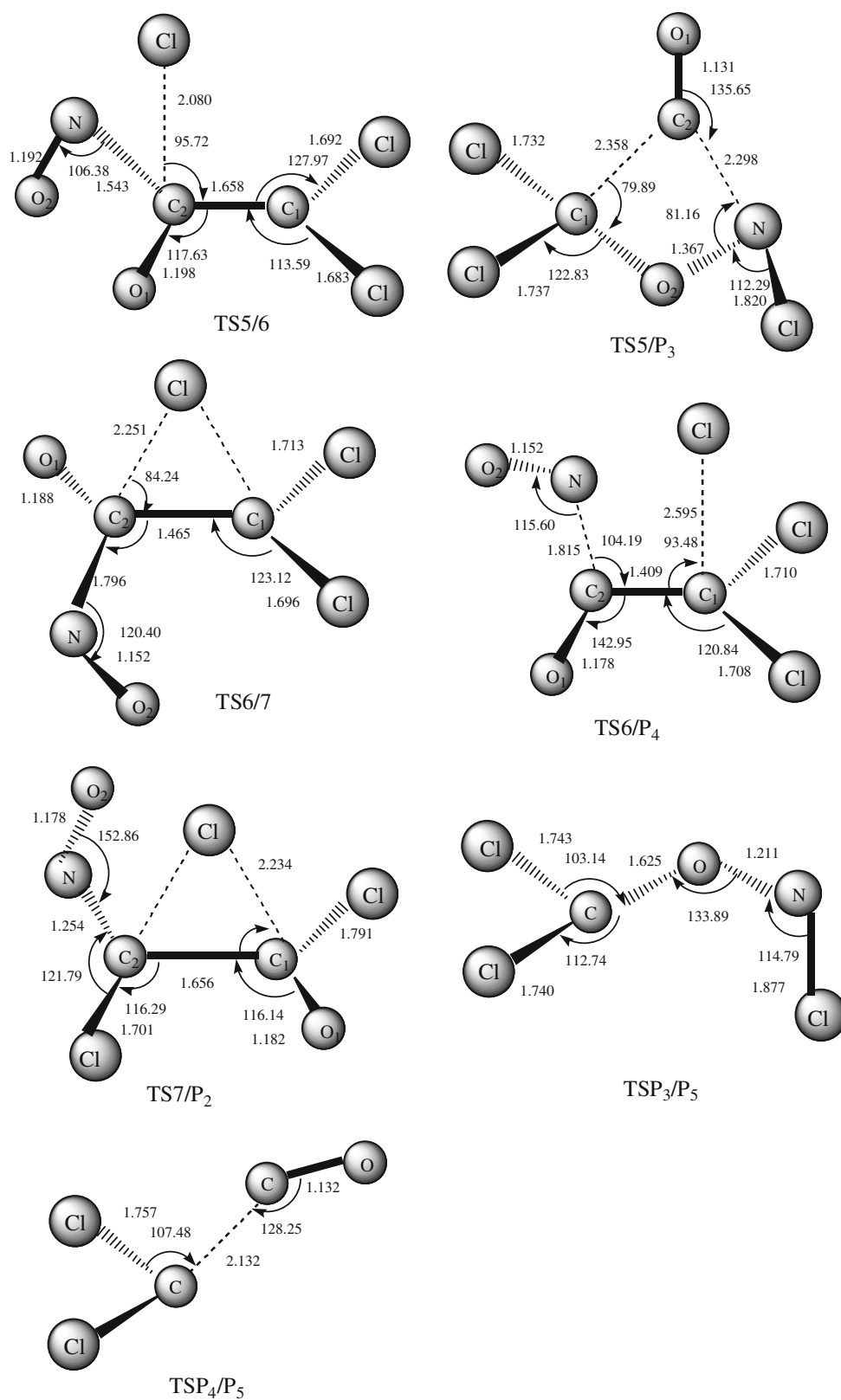
3. Formation pathway of **P**₃ (CO + CCl₂ONCl)

From Fig. 4, we find that only one feasible pathway is associated with the formation of **P**₃, which can be written as



The formation of O-cNCNClOCCl₂ (**5**) is the same as that in path **P**₂(3). Isomer **5** can lead to **P**₃ via the rupture of C1–C2 and C2–N bonds. The barrier for **5** → **P**₃ conversion is 44.1 kcal/mol.

Fig. 3 continued

4. Formation pathways of **P**₄ (CINO + OCCCl₂)

For product **P**₄ (CINO + OCCCl₂), there are two pathways are feasible as follows:

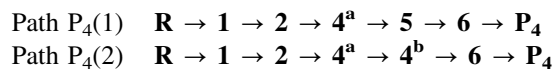


Table 1 The energies of the reactants, products, intermediates and transition states at the B3LYP/6-311G(d,p) and CCSD(T)/6-311+G(d,p)//B3LYP/6-311G(d,p)+ZPVE levels in a.u.

Species	B3LYP	ZPVE		CCSD(T)//B3LYP		Total
Reactant	-1,661.9173449	13.20661	(0.0)	-1,659.5830598	(0.0)	0.0
P₁ (C ₂ Cl ₃ + NO)	-1,662.018373	13.36551	(0.2)	-1,659.692727	(-68.8)	-68.7
P₂ (COCl ₂ + ClNO)	-1,662.025337	14.42035	(1.2)	-1,659.689478	(-66.8)	-65.6
P₃ (CO + ClNOCCl ₂)	-1,661.9457224	12.09791	(-1.1)	-1,659.6218965	(-24.4)	-25.5
P₄ (ClNO + OC ₂ Cl ₂)	-1,662.0121129	13.76599	(0.6)	-1,659.6722459	(-56.0)	-55.4
P₅ (ClNO + CO + CCl ₂)	-1,661.9470114	9.75685	(-3.4)	-1,659.620814	(-23.7)	-27.1
1	-1,661.9975296	16.79417	(3.6)	-1,659.6783056	(-59.8)	-56.2
2	-1,662.0176711	15.20065	(2.0)	-1,659.6941746	(-69.7)	-67.7
3	-1,662.0181788	15.19954	(2.0)	-1,659.6947484	(-70.1)	-68.1
4^a	-1,661.9964925	15.42375	(2.2)	-1,659.6868404	(-65.1)	-62.9
4^b	-1,661.99480	15.38286	(2.2)	-1,659.6861841	(-64.7)	-62.5
5	-1,662.01212	16.12019	(2.9)	-1,659.6919554	(-68.3)	-65.4
6	-1,662.0210521	15.01978	(1.8)	-1,659.7103342	(-79.9)	-78.1
7	-1,662.0424621	15.14919	(1.9)	-1,659.7309409	(-92.8)	-90.9
TS1/2	-1,661.909656	14.61625	(1.4)	-1,659.5902843	(-4.5)	-3.1
TS2/3	-1,662.00725	14.64726	(1.4)	-1,659.6819285	(-62.0)	-60.6
TS2/4^a	-1,661.9427856	13.36769	(0.2)	-1,659.5902843	(-4.5)	-4.4
TS4^a/4^b	-1,661.9905606	15.16735	(2.0)	-1,659.6823832	(-62.3)	-60.4
TS4^a/5	-1,661.9540587	14.13146	(0.9)	-1,659.6353106	(-32.8)	-31.9
TS4^a/P₂	-1,661.9494904	13.94901	(0.7)	-1,659.6238737	(-25.6)	-24.9
TS4^b/6	-1,661.9515557	13.9306	(0.7)	-1,659.630899	(-30.0)	-29.3
TS4^b/P₂	-1,661.960906	14.11156	(0.9)	-1,659.6379604	(-34.5)	-33.5
TS5/6	-1,661.947569	14.03572	(0.8)	-1,659.623184	(-25.2)	-24.3
TS5/P₃	-1,661.9354227	13.16891	(0.0)	-1,659.6169686	(-21.3)	-21.3
TS6/7	-1,661.9635757	13.89981	(0.7)	-1,659.634552	(-32.3)	-31.6
TS6/P₄	-1,661.9619458	13.98035	(0.8)	-1,659.6274137	(-27.8)	-27.1
TS7/P₂	-1,661.9731224	14.41223	(1.2)	-1,659.6381984	(-34.6)	-33.4
TSP₃/P₅	-1,661.9169979	10.78152	(-2.4)	-1,659.5936063	(-6.6)	-9.0
TSP₄/P₅	-1,661.9448667	10.80268	(-2.4)	-1,659.613081	(-18.8)	-21.2

The values in parentheses and total column are relative energies in kcal/mol

Table 2 Energies of the structures on the most favorite channel at CCSD(T)/6-311+G(d,p)//B3LYP/6-311G(d,p)+ZPVE, CCSD(T)/6-311+G(d,p)//B3LYP/6-311+G(d,p)+ZPVE, CCSD(T)/6-311+G(d,p)//MP2/6-311G(d,p)+ZPVE, and G3MP2 levels in a.u.

Species	CCSD(T)//B3LYP/6-311G(d,p)+ZPVE		CCSD(T)//B3LYP/6-311+G(d,p)+ZPVE		CCSD(T)//MP2/6-311G(d,p)+ZPVE		G3MP2	
R	-1,659.5830598	(0.0)	-1,659.5830354	(0.0)	-1,659.5814555	(0.0)	-1,660.0879322	(0.0)
1	-1,659.6783056	(-56.2)	-1,659.6788398	(-56.6)	-1,659.6793804	(-59.5)	-1,660.1825151	(-59.4)
2	-1,659.6941746	(-67.7)	-1,659.6944288	(-67.9)	-1,659.6946403	(-70.9)	-1,660.1995276	(-70.0)
3	-1,659.6947484	(-68.1)	-1,659.6947496	(-68.2)	-1,659.6950655	(-71.2)	-1,660.1960830	(-67.9)
P1	-1,659.6927270	(-68.7)	-1,659.6928835	(-68.8)	-1,659.5876389	(-66.8)	-1,660.1958909	(-67.7)
TS1/2	-1,659.5902843	(-3.1)	-1,659.5904648	(-3.3)	-1,659.6902167	(-4.0)	-1,660.0970007	(-5.7)
TS2/3	-1,659.6819285	(-60.6)	-1,659.682031	(-60.7)	-1,659.6829225	(-64.2)	-1,660.1879180	(-62.7)

The values in parentheses are relative energies in kcal/mol

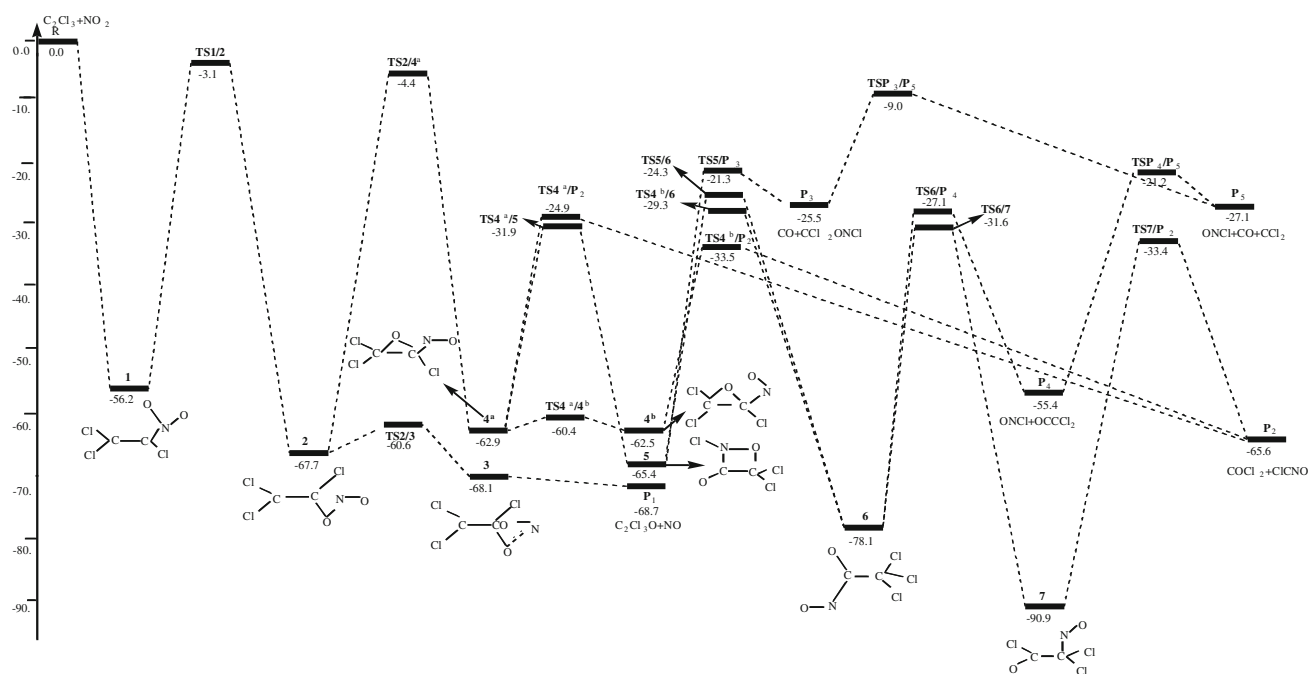


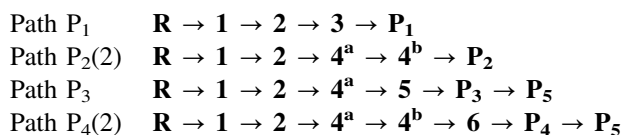
Fig. 4 The sketch map of the potential energy surface (PES)

The formation pathway of $\text{ONC}(\text{O})\text{CCl}_3$ (**6**) has been discussed previously. For brevity, we decide not to discuss it again. **6** can undergo 1,3-Cl shift along with C2–N bond cleavage to generate **P₄**. The barrier height of the step **6** → **P₄** is 51.0 kcal/mol.

Now let us discuss the secondary dissociation pathways of the primary products **P₃** ($\text{CO} + \text{CCl}_2\text{ONCl}$) and **P₄** ($\text{ClNO} + \text{OCCCl}_2$). On the one hand, **P₃** can further dissociate to **P₅** ($\text{ClNO} + \text{CO} + \text{CCl}_2$) via C–O bond rupture with the barrier of 16.5 kcal/mol. On the other hand, **P₄** can dissociate to **P₅** via C–C bond rupture with a barrier of 34.2 kcal/mol.

3.3 Reaction mechanism

On the basis of the reaction pathways obtained in the last section, let us discuss the mechanism of the $\text{C}_2\text{Cl}_3 + \text{NO}_2$ reaction. Here, for easier discussion, the most possible reaction pathways of four primary products **P₁** ($\text{C}_2\text{Cl}_3\text{O} + \text{NO}$), **P₂** ($\text{COCl}_2 + \text{ClCNO}$), **P₃** ($\text{CO} + \text{ClNOCCl}_2$), **P₄** ($\text{ClNO} + \text{OCCCl}_2$) and one secondary product **P₅** ($\text{ClNO} + \text{CO} + \text{CCl}_2$) are listed again:



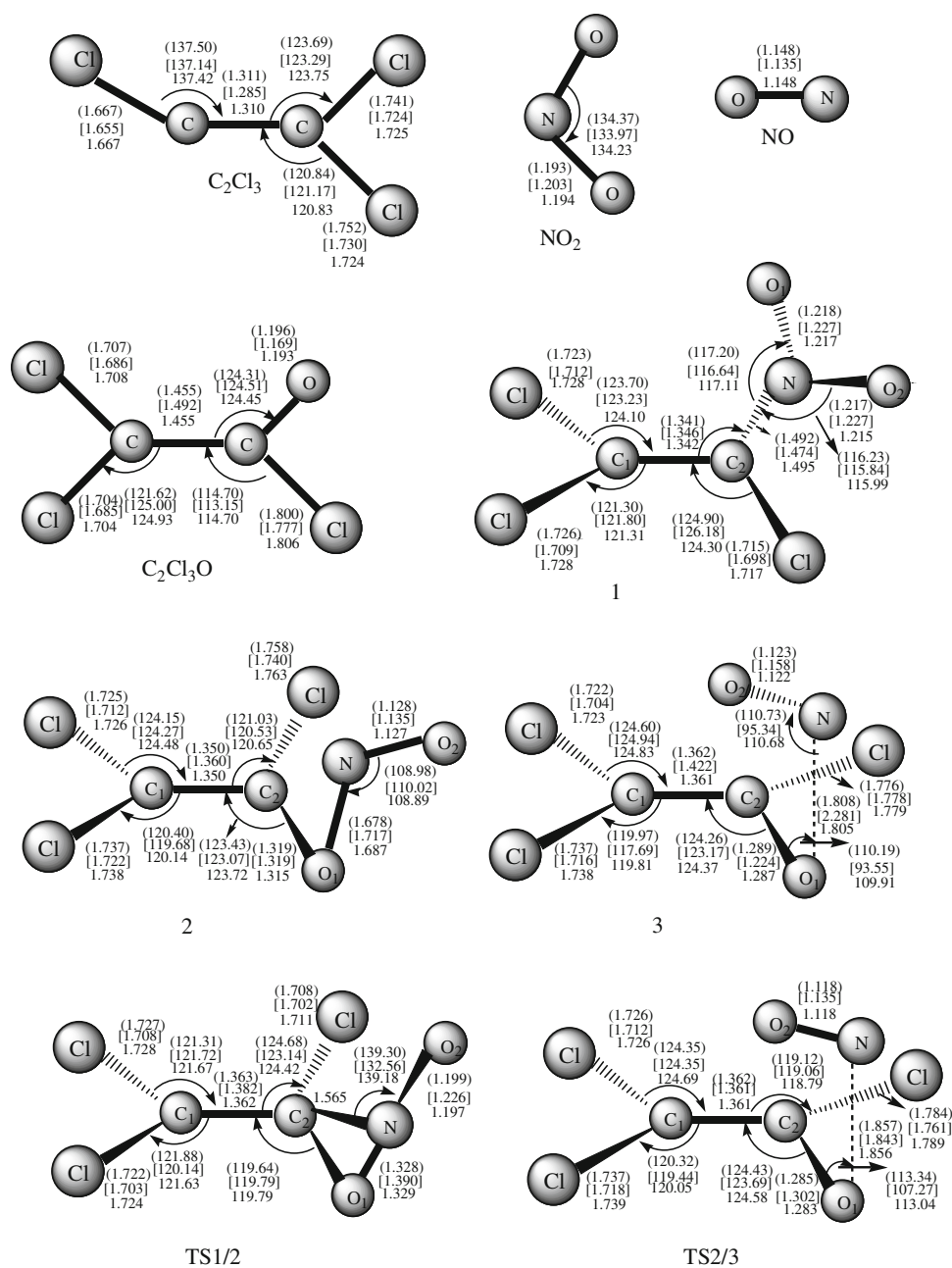
The C_2Cl_3 radical can barrierlessly react with NO_2 at the middle-N site to form intermediate $\text{C}_2\text{Cl}_3\text{NO}_2$ (**1**) followed by isomerization to $\text{C}_2\text{Cl}_3\text{ONO}$ (**2**) which is involved in all

reaction pathways. Starting from **2**, path **P₁** to form product **P₁** is the most favorable pathway since the barrier for step **2** → **3** (7.1) in path **P₁** is much lower than that for **2** → **4^a** (63.3) involved in other three pathways. Much less competitively, because the barrier of **4^b** → **P₂** (29.0) in path **P₂**(2) is smaller than **4^a** → **5** (31.0) and **5** → **P₃** (44.1) in path **P₃** as well as **4^b** → **6** (33.2) and **6** → **P₄** (51.0) in path **P₄**(2), path **P₂**(2) may be kinetically the second feasible pathway followed by **path P₃** and **path P₄**(2) being the last two feasible pathways. When secondary dissociation procedure is considered, some of the primary products **P₃** and **P₄** may lead to **P₅**. As a result, reflected in the final products, **P₁** ($\text{C}_2\text{Cl}_3\text{O} + \text{NO}$) is the major product with a considerable large yields, **P₂** ($\text{COCl}_2 + \text{ClCNO}$) is the second favorable product followed by **P₃** ($\text{CO} + \text{ClNOCCl}_2$) and **P₄** ($\text{ClNO} + \text{OCCCl}_2$) being the third and fourth feasible products, the secondary product **P₅** ($\text{ClNO} + \text{CO} + \text{CCl}_2$) may occupy only a small part.

4 Experimental implication

Now, let us make the comparison between our theoretical results and the available experimental and theoretical studies for the $\text{C}_2\text{Cl}_3 + \text{NO}_2$ reaction. Two experimental investigations by Xiang et al. [10, 11] have reported on the title reaction. Based on their experimental studies, three products Cl_2CO , NO and CO are observed, the detected Cl_2CO , NO and CO can be found as one species of **P₂** ($\text{COCl}_2 + \text{ClCNO}$), **P₁** ($\text{C}_2\text{Cl}_3\text{O} + \text{NO}$), and **P₃**

Fig. 5 The optimized structures of the species involved in the most feasible channel at MP2/6-311G(d,p) (in parentheses) and B3LYP/6-311++G(d,p) (in square brackets) levels



(CO + ClNOCCl₂) and **P₅** (ClNO + CO + CCl₂), respectively. Thus, their experimental results are in good agreement with our theoretical studies.

Recently, a detailed theoretical investigation on the $C_2Cl_3 + NO_2$ reaction has been carried out by Xiang et al. [11]. There are some discrepancies between their results and our theoretical investigations, that is, (1) In Xiang et al.'s studies, two initial adducts IMn1 ($C_2Cl_3-NO_2$) and IM1t (C_2Cl_3-ONO) corresponding to N-attack and O-attack adducts are obtained. In our studies, however, only the N-attack adduct $C_2Cl_3-NO_2$ is obtained. The O-attack adduct C_2Cl_3-ONO which presents a planar structure, is in fact a first-order saddle point because it has one imaginary

frequency. We attempted to obtain a true O-attack adduct with planar structure, but failed because in all cases we obtained structure **2** C_2Cl_3-ONO whose optimized geometry shows steric effects between C_2Cl_3O and NO. In addition, we note that IM1t obtained by Xiang et al. is more like the adduct species between CCl_2CO and NO rather than the one between C_2Cl_3 and NO_2 . Moreover, to our best knowledge, for the reactions between a chlorinated hydrocarbon species (e.g., $CHCl_2$, CCl_3 , CH_2F , CH_2Cl , CHF , $CHCl$) [18, 19, 24, 35, 37] and NO_2 , the end-N attack is the exclusive feasible entrance channel. Therefore, IM1t with planar structure is not shown in our results. (2) Based on Xiang et al.'s studies, IM1c can dissociate to

$C_2Cl_3O + NO$ with no transition state involved. However, a transition state **TS2/3** and a weakly bond complex **3** are obtained in our studies. Moreover, the existence of **TS2/3** and **3** are confirmed by additional calculations at B3LYP/6-311++G(d,p), and MP2/6-311G(d,p) levels. (3) In Xiang et al.'s studies, only the chainlike structures are considered. Although their potential energy surface for $C_2Cl_3 + NO_2$ reaction can well explain the experimental observations, their calculations are incomplete. For example they do not consider cyclic intermediates. In the present paper, we focus our main attention on the cyclic intermediates as well as their further changes. In view of there is the marked discrepancy between the two theoretical studies, future reinvestigation of the title reaction is therefore very desirable.

5 Assessment of computational reliability

In order to further confirm the reliability of the B3LYP/6-311G(d,p) structures, we performed test calculations on the species **R** ($C_2Cl_3 + NO_2$), **1** ($C_2Cl_3NO_2$), **2** (C_2Cl_3ONO), **3** ($C_2Cl_3O...NO$), **TS1/2**, **TS2/3**, and **P₁** ($C_2Cl_3O + NO$) which are involved in the most favorite channel at the B3LYP/6-311++G(d,p), and MP2/6-311G(d,p) levels, followed by the CCSD(T)/6-311+G(d,p) energy calculations. As shown in Fig. 5, the structural parameters at three levels are generally in good agreement with each other. We expect that the B3LYP/6-311G(d,p) method is reliable for description of the structures for the title reaction.

In addition, the more composite G3MP2 calculations are carried out on the above seven species. As shown in Table 2, the calculated relative energies at the four levels are generally in consistent with each other. The largest deviation of CCSD(T)//B3LYP/6-311G(d,p)+ZPVE with CCSD(T)//B3LYP/6-311++G(d,p)+ZPVE, CCSD(T)//B3LYP/6-311G(d,p)+ZPVE and G3MP2 are 0.4 kcal/mol for **1**, 4.0 kcal/mol for **TS2/3** and 3.2 kcal/mol for **1**, respectively. In all, the CCSD(T)//B3LYP/6-311G(d,p) method can provide reliable mechanistic information for the radical-molecule reaction of $C_2Cl_3 + NO_2$.

6 Conclusion

The radical-molecule reaction of $C_2Cl_3 + NO_2$ is explored at the B3LYP/6-311G(d,p) and CCSD(T)/6-311+G(d,p) (single-point) levels. The main results can be summarized as follows: (1) This reaction proceeds mostly through singlet pathways and less through triplet pathways. (2) The title reaction is most likely initiated by the carbon (with only one Cl atom)-to-nitrogen approach to form adduct **1** ($C_2Cl_3NO_2$) with no barrier. Subsequently, via a variety of transformation

of isomer **1**, four kinds of primary products **P₁** ($C_2Cl_3O + NO$), **P₂** ($COCl_2 + ClCN$), **P₃** ($CO + ClNOCCl_2$), **P₄** ($ClNO + OCCl_2$) and one secondary product **P₅** ($ClNO + CO + CCl_2$) are obtained. Among these products, **P₁** is the most favorable product, **P₂** and **P₃** are the second and third feasible products, respectively, whereas **P₄** is kinetically the least possible product. In addition, the secondary product **P₅** may have a small amount.

Acknowledgment This work is supported by the National Natural Science Foundation of China (No. 20773048).

References

- Valeiras H, Gupta AK, Senkan SM (1984) *Combust Sci Technol* 36:123. doi:10.1080/00102208408923729
- Senkan SM, Robinson JM, Gupta AK (1983) *Combust Flame* 49:305. doi:10.1016/0010-2180(83)90173-6
- Chang WD, Senkan SM (1989) *Environ Sci Technol* 23:442. doi:10.1021/es00181a009
- Taylor PH, Tirey DA, Dellinger B (1996) *Combust Flame* 104:260. doi:10.1016/0010-2180(95)00117-4
- Taylor PH, Tirey DA, Rubey WA, Dellinger B (1994) *Combust Sci Technol* 101:75. doi:10.1080/00102209408951867
- Russell JJ, Seetula JA, Gutman D, Senkan SM (1989) *J Phys Chem* 93:1935
- Xiang TC, Liu KH, Zhao SL, Su HM, Kong FN, Wang BS (2007) *J Phys Chem A* 111:9606. doi:10.1021/jp074058c
- Wang H, Li JC, Song XL, Li YZ, Hou H, Wang BS, Su HM, Kong FN (2006) *J Phys Chem A* 110:10336. doi:10.1021/jp0633345
- Kostina KS, Bryukov MG, Shestov AA, Knyazev VD (2003) *J Phys Chem A* 107:1776. doi:10.1021/jp027162x
- Xiang TC, Liu KH, Su HM (2007) *Chin. J Chem Phys* 20:407
- Liu KH, Xiang TC, Wu WQ, Zhao SL, Su HM (2008) *J Phys Chem A* 112:10807. doi:10.1021/jp8031034
- Mikhail GB, Sofya AK, Vadim DK (2003) *J Phys Chem A* 107:6574. doi:10.1021/jp034205g
- Baren RE, Erickson MA, Hershberger JF (2002) *Int J Chem Kinet* 34:12. doi:10.1002/kin.10013
- Rim KT, Hershberger JF (1998) *J Phys Chem A* 102:4592. doi:10.1021/jp981362k
- Myerson AL (1975) In: 15th international symposium on combustion. The Combustion Institute, Pittsburgh, PA, p 1085
- Song YH, Blair DW, Siminski VJ, Bartok W (1981) In: 18th international symposium on combustion. The Combustion Institute, Pittsburgh, PA, p 53
- Chen SL, McCarthy JM, Clark WD, Heap MP, Seeker WR, Pershing DW (1986) In: 21st international symposium on combustion. The Combustion Institute, Pittsburgh, PA, p 1159
- Zhang JX, Li ZS, Liu JY, Sun CC (2006) *J Comput Chem* 27:894. doi:10.1002/jcc.20397
- Zhang JX, Li ZS, Liu JY, Sun CC (2007) *Theory Chem Acc* 117:579. doi:10.1007/s00214-006-0244-8
- Eskola AJ, Geppert WD, Rissanen MP, Timonent RS, Halonen L (2005) *J Phys Chem A* 109:5376. doi:10.1021/jp050441a
- Zhang JX, Liu JY, Li ZS, Sun CC (2005) *J Comput Chem* 26:807. doi:10.1002/jcc.20217
- Yamada F, Slagle IR, Gutman D (1981) *Chem Phys Lett* 83:409. doi:10.1016/0009-2614(81)85490-5
- Wollenhaupt M, Crowley JN (2000) *J Phys Chem A* 104:6429. doi:10.1021/jp0005726

24. Zhang JX, Li ZS, Liu JY, Sun CC (2006) *J Comput Chem* 27:661. doi:[10.1002/jcc.20380](https://doi.org/10.1002/jcc.20380)
25. Seidler V, Temps F, Wagner HG, Wolf M (1989) *J Phys Chem* 93:1070. doi:[10.1021/j100340a011](https://doi.org/10.1021/j100340a011)
26. Darwin D, Moore CB (1995) *J Phys Chem* 99:13467. doi:[10.1021/j100036a022](https://doi.org/10.1021/j100036a022)
27. Liu JJ, Ding YH, Yu GT, Feng JK, Sun CC (2002) *J Comput Chem* 23:1031. doi:[10.1002/jcc.10075](https://doi.org/10.1002/jcc.10075)
28. Wagal SS, Carrington T, Filseth SV, Sadowski CM (1982) *Chem Phys* 69:61. doi:[10.1016/0301-0104\(82\)88132-9](https://doi.org/10.1016/0301-0104(82)88132-9)
29. Rim KT, Hershberger JF (1998) *J Phys Chem A* 102:4592. doi:[10.1021/jp981362k](https://doi.org/10.1021/jp981362k)
30. Yu GT, Ding YH, Li ZS, Huang XR, Sun CC (2001) *J Phys Chem A* 105:3388. doi:[10.1021/jp003717h](https://doi.org/10.1021/jp003717h)
31. Yu GT, Ding YH, Li ZS, Huang XR, Sun CC (2001) *J Phys Chem A* 105:9598. doi:[10.1021/jp012481u](https://doi.org/10.1021/jp012481u)
32. Van Hoeymissen J, De Boelpaep I, Uten W, Peeters J (1994) *J Phys Chem* 98:3725. doi:[10.1021/j100065a030](https://doi.org/10.1021/j100065a030)
33. Yu GT, Ding YH, Liu JY, Li ZS, Huang XR, Sun CC (2001) *J Comput Chem* 22:1907. doi:[10.1002/jcc.1141](https://doi.org/10.1002/jcc.1141)
34. Cookson JL, Hancock G, Mckendrick KG, Bunsenges Ber (1985) *Phys Chem* 89:335. doi:[10.1021/j100248a031](https://doi.org/10.1021/j100248a031)
35. Zhang JX, Liu JY, Li ZS, Sun CC (2004) *J Comput Chem* 25:1888. doi:[10.1002/jcc.20121](https://doi.org/10.1002/jcc.20121)
36. Baren RE, Erickson MA, Hershberger JF (2002) *Int J Chem Kinet* 34:12. doi:[10.1002/kin.10013](https://doi.org/10.1002/kin.10013)
37. Zhang JX, Liu JY, Li ZS, Sun CC (2004) *J Comput Chem* 25:1184. doi:[10.1002/jcc.20043](https://doi.org/10.1002/jcc.20043)
38. Geppert WD, Eskola AJ, Timonen RS, Halonen L (2004) *J Phys Chem A* 108:4232. doi:[10.1021/jp0370167](https://doi.org/10.1021/jp0370167)
39. Du BN, Zhang WC (2006) *J Mol Struct THEMCHEM* 801:39
40. Frisch MJ, Trucks GW, Schlegel HB et al (1998) *Gaussian 98, Revision A.6*. Gaussian, Inc, Pittsburgh, PA